The Journal of Experimental Biology 204, 823–834 (2001)
Printed in Great Britain © The Company of Biologists Limited 2001
JEB3069

Ca^{2+} IN SPECIFICATION OF VEGETAL CELL FATE IN EARLY SEA URCHIN EMBRYOS

I. YAZAKI

Department of Biological Science, Tokyo Metropolitan University, Minamiohsawa1-1, Hachiohji, Tokyo 192-0397, Japan

e-mail: yazaki-ikuko@c. metro-u.ac. jp

Accepted 1 December 2000; published on WWW 12 February 2001

Summary

In sea urchin embryos, the first specification of cell fate occurs at the fourth cleavage, when small cells (the micromeres) are formed at the vegetal pole. The fate of other blastomeres is dependent on the receipt of cell signals originating from the micromeres. The micromeres are fated to become skeletogenic cells and show the ability to induce the endoderm (the archenteron) in the neighbouring cells during the 16- to 60-cell stage. Several molecules involved in signaling pathways, i.e. Notch for mesoderm specification, bone morphogenic protein (BMP) for ectoderm specification and β-catenin for endoderm specification, are spatially and temporally expressed during development. In the micromeres, β-catenin increases and subsequently localizes to the nuclei under the regulation of TCF, a nuclear binding partner of β-catenin, until the 60-cell stage. However, the mechanisms activating these signaling substances are still unclear. In this article, I demonstrate some specific properties of the membrane and cytoplasm of micromeres including new findings on intracellular Ca^{2+} concentration, and propose a mechanism by which the functional micromeres are autonoumously formed. The possible roles of these in the specification of vegetal cell fate in early development are discussed.

Key words: Sea urchin, Embryo, Micromere, Ca^{2+}, Endoplasmic reticulum accumulation, Cell specification.

Specification of cell fate in early sea urchin embryos

It is well-known that during the early development of sea urchin embryos, the fate of a particular cell depends on its position in the embryo, rather than on the cytoplasm it has acquired from the egg. It was shown (Driesch, 1900) that, if isolated, every blastomere up to the 4-cell stage was able to form a small but complete pluteus larva (Fig. 1I, J). The third division occurs at right angles to the first and second cleavage planes (Fig. 1A–C). If an embryo is bisected along the first or second cleavage plane, each half forms a small but complete larva. If the embryo is bisected along the third cleavage plane, however, the result is different; one half forms a dwarf larva but the other develops into a hollow, ciliated blastula-like embryo (Fig. 1E) (Horstadius, 1939). This means that the four blastomeres at the 4-cell stage are equivalent and regulative, but by the next division the blastomeres are segregated into cells with different potentialities. This differential ability has been recognized in unfertilized eggs. There is no visible marker to indicate the polarity of sea urchin eggs but such a marker is present in the extracellular structure surrounding the eggs, the jelly layer. The position of the jelly canal in this transparent jelly coat marks the future animal pole of the embryo (Boveri, 1901). When the jelly canal was visualized using carbon particles and the unfertilized egg bisected into animal and vegetal halves before insemination, it was found that the animal half developed into a blastula-like larva and the vegetal half became an almost normal larva (Maruyama et al., 1985).

At the fourth division, the cells occupying the animal half of the embryo divide equally, while in the vegetal half unequal divisions occur, so that three different sizes and qualities of blastomere are formed: the mesomeres, the macromeres and the micromeres (Fig. 1D). The tiers of blastomeres located along the animal–vegetal (A–V) axis are fated to give rise to the ectoderm, the endoderm and the mesoderm, and are specified and patterned by the coordinated action of localized, maternally derived determinants and cell–cell signals (Horstadius, 1939). The A–V axis is further patterned to produce five distinct territories by the 60-cell stage that are specified by a signal transduction cascade initiatiated by the micromeres (Davidson, 1989).

Signal molecules or determinant molecules involved in the specification of sea urchin embryonic cells have recently been found. Transcripts of bone morphogenic protein (BMP) gene of sea urchin, which first appear in the oral ectoderm region at about the 200-cell stage, suppress the commitment of cells to vegetal fates (Angerer et al., 2000). The oral ectoderm occupies an epithelial region surrounded by four arms of a pluteus including a mouth, and is distinct from the aboral ectoderm, the dorsal and the ventral epithelium (Fig. 1I,J). Specification of the fate of secondary mesenchyme cells (SMC in Fig. 1G)

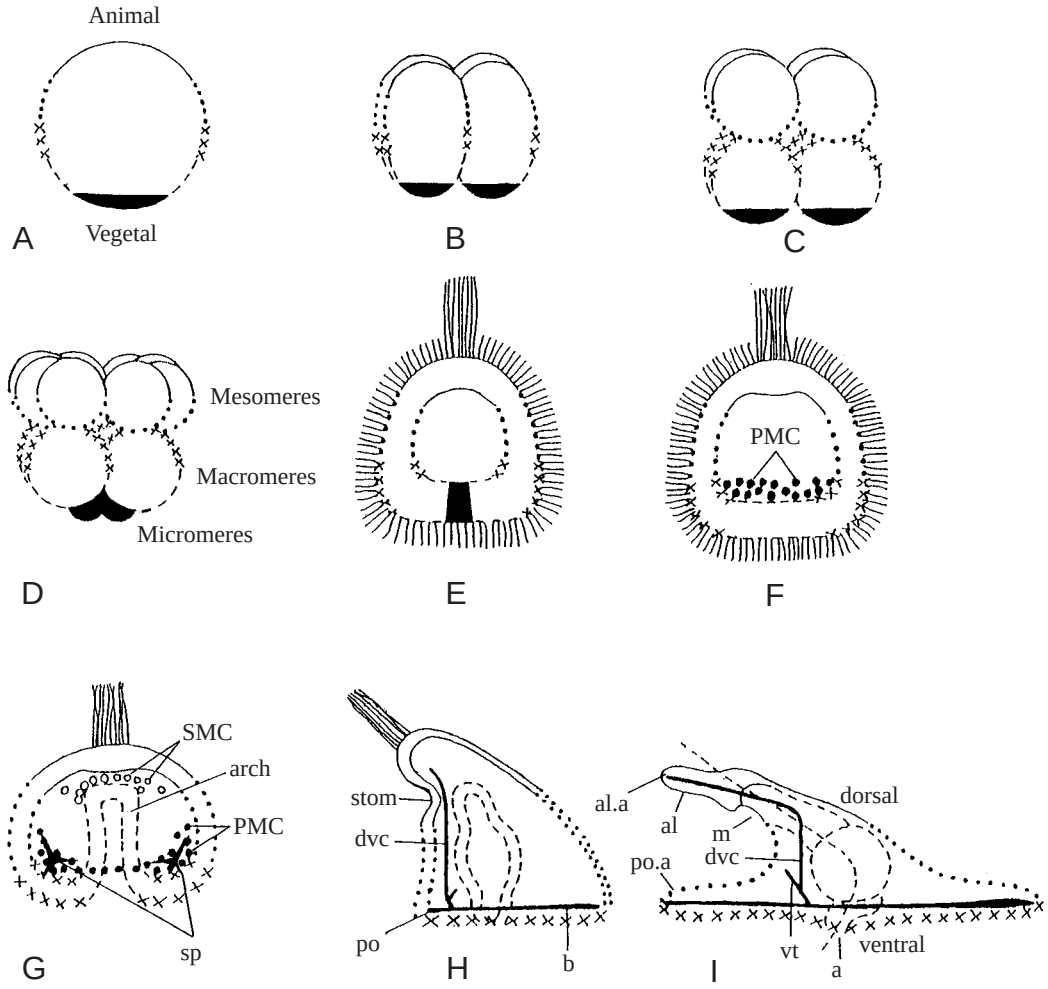

Fig. 1. Diagram of the normal development of a sea urchin embryo. Regions of the embryos that form mesomeres are shown with continuous and dotted lines; within the macromeres, membrane areas marked with crosses become ectoderm while those marked with a broken line become endoderm; the micromeres, coloured black, form skeletogenic cells. (A) Uncleaved egg. (B) 4-cell stage. (C) 8-cell stage. (D) 16-cell stage. (E) Blastula. (F) Mesenchyme blastula after the formation of the primary mesenchyme cells (PMC). (G) Gastrula; the secondary mesenchyme cells (SMC) are liberated from the tip of the archenteron (arch) and the two triradiate spicules (sp) have formed. (H) Prism stage; stomodaeum (stom) is invaginating and skeletal rods are growing. b, body rod; dvc, dorsoventral connecting rod; po, post-oral rod. (I) Pluteus larva from the left side; the broken line indicates the position of the egg axis. (J) Pluteus larva from the ventral side. a, anus; al, anterolateral rod; al.a, anterolateral arm; m, mouth; po.a, postoral arm; vt, ventral transverse rod. (Modified with permission from Horstadius, 1939.)

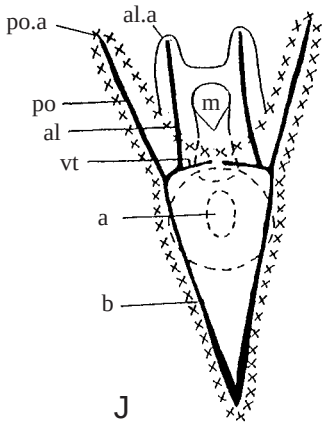

in the endoderm involves the Notch signaling pathway in which the Notch receptor, a membrane protein, is expressed from the 120-cell stage and decreases the number of endodermal cells formed by causing the production of SMC (Sherwood and McClay, 1999). β-catenin, which is involved in the Wnt pathway, initially increases in the micromeres at the 16-cell stage and then accumulates in the vegetal nuclei to specify the endoderm (Logan et al., 1999). The β-catenin is regulated by a ternary complex factor (TCF), a binding partner of nuclear β-catenin, until the 60-cell stage (Vonica et al., 2000). While these facts are very interesting it is still not known how the signals are activated, or what physiological conditions in cells regulate these signal pathways. In this paper I discuss morphological and physiological cell functions that may be involve in the autonomous specification of the micromeres.

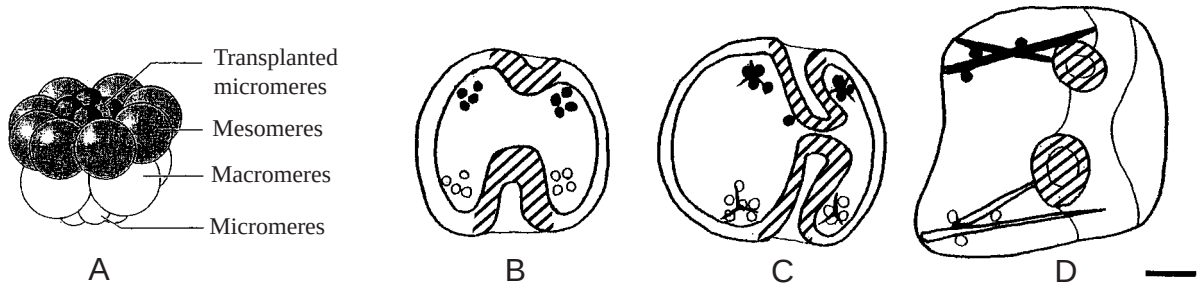

Fig. 2. Micromere transplantation experiment. (A) Transplanted micromeres previously labelled with the fluorescent dye, rhodamine B isothiocyanate, are removed from a donor embryo and then placed at the animal pole of a host embryo. (B) The resulting chimeric embryo gastrulates from both the animal and vegetal poles. (C) The labelled and host primary mesenchyme cells ingress, and form spicules. (D) Pluteus stage equivalent larva shows two sets of spicules and two guts that each differentiate into the three parts of the digestive tract. The hatched areas show the differentiated regions as demonstrated by whole-mount *in situ* hybridization using a probe for the gut-specific marker gene, Endo 16. Scale bar, 20 μm. (Modified with permission from Ransick and Davidson, 1993.)

Autonomous specification of micromeres

The first specification of blastomeres occurs autonomously in the micromeres at the 16-cell stage, and the first signals in embryos are sent out from these micromeres to the neighbouring cells, the macromeres, to induce the archenteron (Fig. 1G). The micromeres self-differentiate to the primary mesenchyme cells (PMC, Fig. 1F), and form the larval spicules (Fig. 1G) and skeletal rods (Fig. 1H–J). If the micromeres are removed from 16-cell stage embryos and cultured in isolation, they form mesenchymal aggregates, which subsequently differentiate into skeletogenic cells, as in normal embryos (Okazaki, 1975). The inductive ability of the micromeres has been demonstrated by transplantation experiments (Horstadius, 1939; Ransick and Davidson, 1993) showing that if extra micromeres were transplanted onto the mesomeres, a second archenteron invaginated from the animal pole, in addition to the original archenteron, which invaginates from the vegetal pole of the host embryo (Fig. 2). Experiments in which micromeres were removed at various stages suggested that contact with micromeres during the 16- to 60-cell stage was necessary for normal induction of the archenteron (Ransick and Davidson, 1995).

Electrical coupling is initially established between the micromeres and macromeres at the 16-cell stage. The maximum junctional conductance of 26 nS decreases to 13 nS in the latter half of the cell cycle and coupling is finally lost before the next division (2 in Fig. 3). In most cases, some electrical coupling remains after each cleavage via the cytoplasmic bridges that connect newly divided sister cells, but this later disappears (1, 3, 4 in Fig. 3). The electrical coupling is reestablished between the micromeres and the neighbouring macromeres after the fifth and sixth divisions, although the cells of these pairs are not sisters (5 in Fig. 3). There is no significant coupling between other pairs of blastomeres up to the 60-cell stage. Intercellular current intensity is independent of transjunctional voltage, nondirectional and sensitive to 1-octanol, indicating that it is gated through gap-junction channels. However, when a fluorescent dye, Lucifer Yellow,

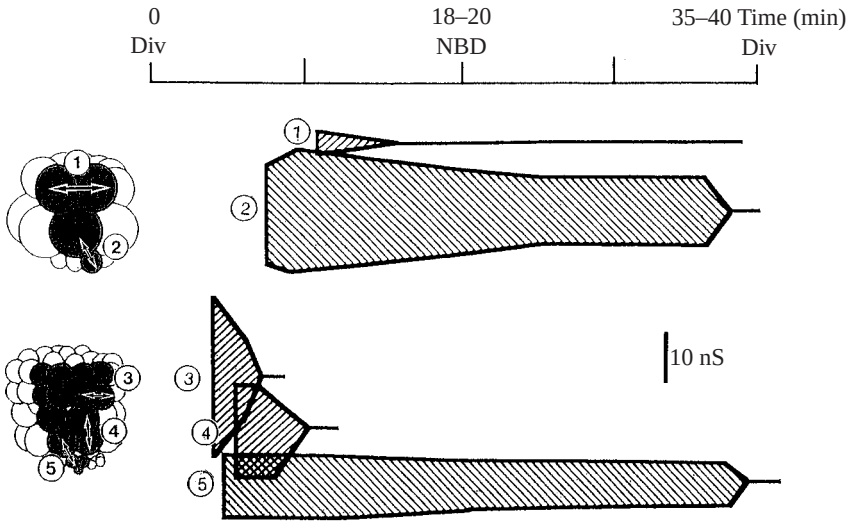

Fig. 3. Electrical coupling in 16- to 60-cell stage sea urchin embryos of *Paracentrotus lividus*. To measure electric communication, two patch pipettes in the whole-cell voltage-clamp configuration were applied independently to two adjacent blastomeres (arrows). Cells were voltage-clamped at −80 mV. The magnitude of the junctional conductance between blastomeres is indicated by the width of the shaded area (vertical scale bar, 10 nS) during one cleavage division (Div; horizontal axis). NBD, nuclear breakdown. Cell pairs selected for recording are numbered 1–5; 1 and 2 are sister cells at the 16-cell stage. Recording 1 is from mesomere/mesomere coupling, recording 2 from macromere/micromere coupling. Recordings 3–5 are all from the 60-cell stage. Cells 3 and 4 are sister cells but 5 is not. Recording 3 shows coupling between mesomere descendants, 4 shows coupling between macromere descendants and 5 shows coupling between a descendant of a macromere and a larger micromere. Data from the 32-cell stage are omitted. (Taken from Yazaki et al., 1999.)

is injected into individual blastomeres it does not diffuse between any of the blastomeres. Diffusion of the dye is only recognized after the seventh division (120-cell stage) and is independent of cell type. Since a significant delay in the formation of the archenteron is induced in embryos treated with 1-octanol during the 16- to 60-cell stages, electrical communication between blastomeres may play a role in embryonic induction by the micromeres (Yazaki et al., 1999). If the micromeres are deleted from the embryos, invagination of the archenteron is markedly delayed, although the descendants of macromeres finally form not only the archenteron but also the skeleton, instead of the deleted micromeres (Horstadius, 1939).

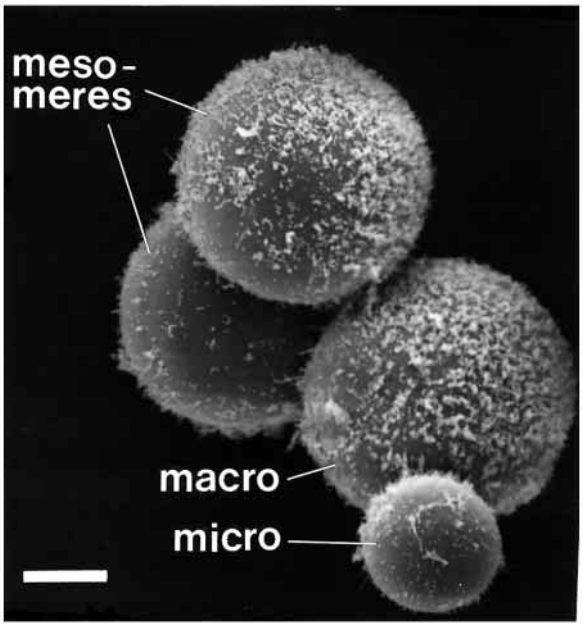

Fig. 4. A scanning electron micrograph showing the natural configuration of two mesomeres, one macromere (macro) and one micromere (micro) in a quarter sea urchin embryo at the 16-cell stage. The apical areas of the mesomeres and macromere are organized into microvilli, whereas the basal regions are smooth. The micromere has few microvilli. Scale bar, 10 μm. (Taken from Dale et al., 1997, with permission).

Micromere formation and properties

The plasma membrane and cortical layer of micromeres

The plasma membrane of the micromeres is distinguished from that of other blastomeres by its smooth surface (Fig. 4) and its specific electrophysiological characteristics (Fig. 7, Table 1). The surface membrane of the zygote is microvillous. When the zygote divides, the resulting blastomeres have two distinct membrane regions: one is the egg-derived villous region (the apical membrane furthest away from the cleavage furrow) and the other a newly formed smooth region (the basal membrane adjoining the cleavage furrow). The blastomeres never adhere to other cells at the apical membrane area. When two blastomeres are adjacent at the apical membrane region, the two cells independently develop into separate larvae, whereas if they are adjacent at the basal membrane region, they form one larva by association of the two cells (Kuraishi, 1989). An egg surface-specific antibody purified by immunological absorption with eggs from different species has been shown to stain the apical membrane, but does not stain the basal membrane (Yazaki, 1984; Yazaki and Uemura, 1989). After furrowing is completed, shrinkage of the cortical network of actin filaments lining the original egg membrane occurs so that the basal membrane in the cleavage plane is an area of smooth membrane without either microvilli or a cortical actin network (Yazaki, 1991). The appearance of the micromere membrane and the fact that only a small area of it binds the egg surface-specific antibody shows that it is mainly composed of basal membrane, which differs from both the apical membrane and its underlying cortical structures.

The micromeres of sea urchins *Arbacia punctulata* and *Hemicentrotus pulcherrimus* lack the cortical pigment granules that occur in other blastomeres (Dan, 1954; Dan, 1960). In both mesomeres and macromeres of the 16-cell stage embryos, cortical pigment granules line the outward-facing surfaces but do not occur on the interblastomeric surfaces. Movements of

Table 1. *Electrophysiological properties of the micromere*

Cell origin	Cell diameter (μm)	Conductance (pS μm^{-2})	Resting potential (mV)	Ca^{2+} currents (μA cm^{-2})
2-cell stage	70	2.0±0.1 (30)		
4-cell stage	53	3.5±0.2 (17)	–28±2	8.5±1.2 (3)
8-cell stage	43	4.1±0.1 (25)	–24±3	5.4±1.5 (5)
16-cell stage				
Mesomere	31	7.6±0.5 (20)	–25±3	7.4±1.7 (5)
Macromere	37	5.1±0.4 (13)	–27±4	2.3±1.2 (5)
Micromere	20	16.7±1.1 (20)	–9±1	0 (5)

Specific steady-state conductance, resting potential and L-type Ca^{2+} currents in blastomeres are compared at various cell stages of sea urchin *Paracentrotus lividus* embryos.

The Ca^{2+} currents generated at +20 mV from a holding potential of –30 mV are expressed per cm^2.

Values are means ± S.E.M. (*N*).

Data are taken from Dale et al., 1997, with permission.

pigment granules from the vegetal pole are initiated at the 2- to 4-cell stages and can be arrested by microfilament inhibitors (Belanger and Rustad, 1972). This observation suggests that the properties of the micromere membranes are specified by cortical movements from the vegetal to the animal pole, in addition to the formation of new membrane at each cleavage, as described above.

Using the whole-cell clamp technique, it was found that L-type Ca^{2+} channels are present in early sea urchin blastomeres, and that these are activated during M-phase and subsequently inactivated in S-phase of the mitotic cycle (Fig. 5). Fragmentation experiments, in which blastomeres were divided into apical and basal regions before patch clamping, show that the calcium channels are clustered in the apical membrane (Fig. 6). Meanwhile, the specific steady-state conductance, detected as K^+ efflux, is approximately twofold higher in the basal membrane than in the apical membrane (Yazaki et al., 1995). The finding that cytochalasin B inhibits cyclic activity in both the M- and S-phases, while colchicine inactivates the L-type current in M-phase and activates a large T-type calcium current in the S-phase, suggests that channel behaviour is regulated by cytoskeletal elements (Yazaki et al., 1995). In parallel with the increase in basal membrane area as division progresses, the calcium currents in M-phase decrease from 8.5 μA cm^{-2} at the 4-cell stage to 5.4 μA cm^{-2} at the 8-cell stage. In 16-cell stage embryos, calcium currents are 7.4 μA cm^{-2} in the mesomeres, 2.3 μA cm^{-2} in the macromeres, and are not detected in the micromeres, in keeping with the fact that this plasma membrane is derived from basal membrane (Fig. 7, Table 1). The micromeres do, however, have a two- to threefold higher specific steady state conductance than either the mesomeres or the macromeres, suggesting that many more K^+ channels are present in the micromeres than in the other blastomeres (Table 1).

Vegetal accumulation of the endoplasmic reticulum occurs during micromere formation

Unequal division is preceded by migration of the nucleus towards the cell periphery at the vegetal pole at the 8-cell stage, when a hemicentric mitotic apparatus is formed. This gives rise to unequal blastomeres, the macromere and the micromere (Dan, 1979; Dan et al., 1983). If embryos are exposed to a 10-minute pulse of the surfactant, sodium dodecyl sulphate (SDS) during the 4-cell stage, both nuclear migration and micromere formation are inhibited. The SDS-treated embryos, which have 16 equal-sized blastomeres, are capable of development but show a decrease in the number of mesenchyme cells, have defective skeletons and show retardation or inhibition of gastrulation (Tanaka, 1976; Tanaka, 1979).

After the 8-cell stage in Ascidians, there are three successive unequal divisions in the posterior region, which always

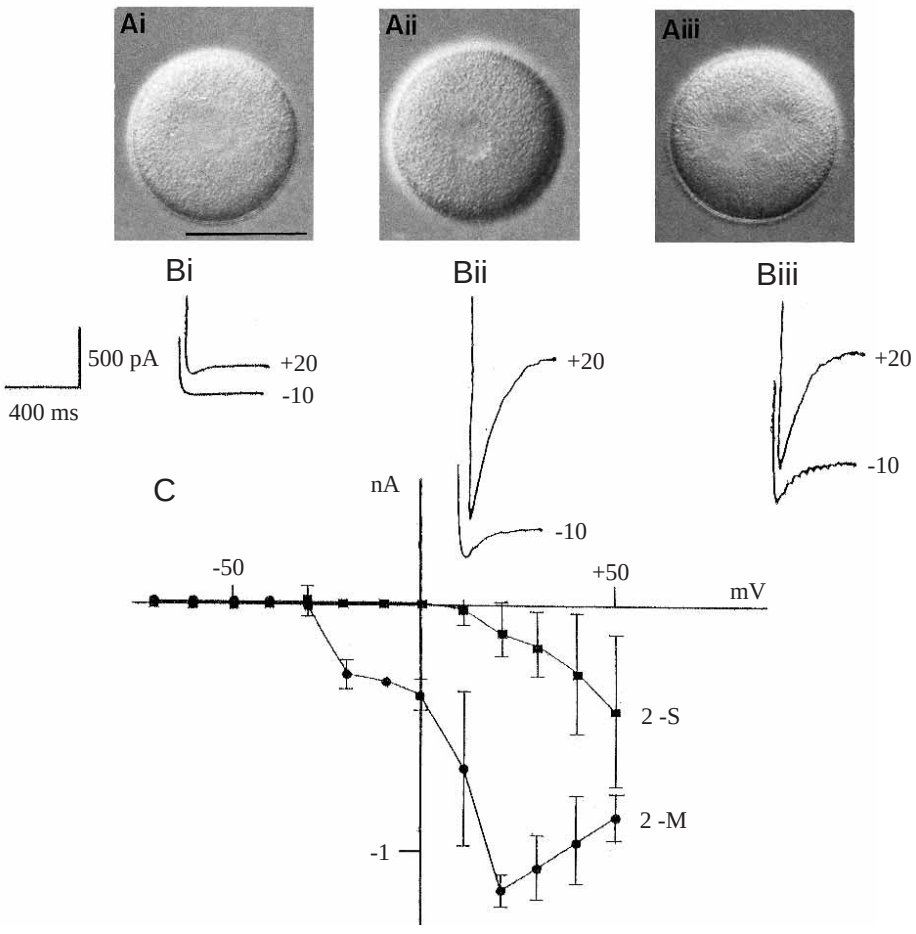

Fig. 5. L-type Ca^{2+} currents and the cell cycle in early embryos of the sea urchin *Paracentrotus lividus*. Cell cycle events were followed under a light microscope. (Ai–Aiii) A blastomere at the 2-cell stage. Whole-cell currents were recorded in S-phase (Ai; intact nuclear membrane) and M-phase (Aii, Aiii; between nuclear membrane breakdown and cytokinesis). Scale bar, 50 μm. (Bi–Biii) Typical leak-subtracted currents in 2-cell stage blastomeres at the phases of the cell cycle indicated in Ai, Aii and Aiii, respectively. The cells were clamped at a holding potential of −80 mV and step-depolarized for 400 ms to the voltage indicated. (C) Current/voltage relationships for the L-type Ca^{2+} currents from 2-cell stage blastomeres in S-phase (squares; 2-S) and M-phase (circles; 2-M). Values are means + S.E.M. of 12 separate experiments. (Taken from Yazaki et al., 1995, with permission.)

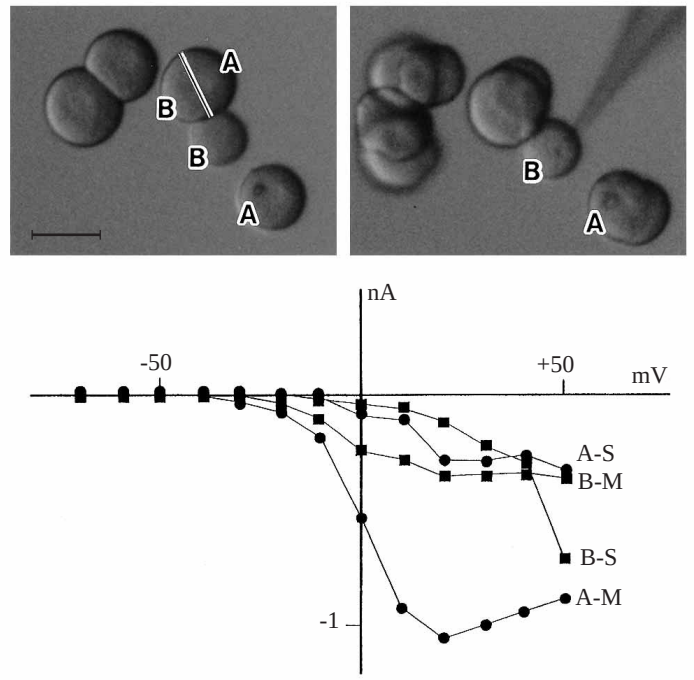

Fig. 6. L-type Ca^{2+} currents in apical and basal fragments of 4-cell stage blastomeres of *Paracentrotus lividus*. The bottom right blastomere was cut using a glass needle into two fragments: an anucleated basal fragment (B) and a nucleated apical fragment (A). The sister blastomere of the fragments (A,B) is marked with a line to indicate the cutting plane that generated A and B. Fragment A and the remaining three blastomeres cleaved following recording (right-hand frame). Scale bar, 50 μm. The fragments were voltage-clamped at a holding potential of –80 mV and step-depolarized for 400 ms to the voltages indicated. Values for the current/voltage relationship of the currents from the apical (A) and the basal (B) fragments in S-phase (A-S, B-S) and in M-phase (A-M, B-M) are the means of three separate experiments; error bars are omitted for clarity. (Taken from Yazaki et al., 1995, with permission.)

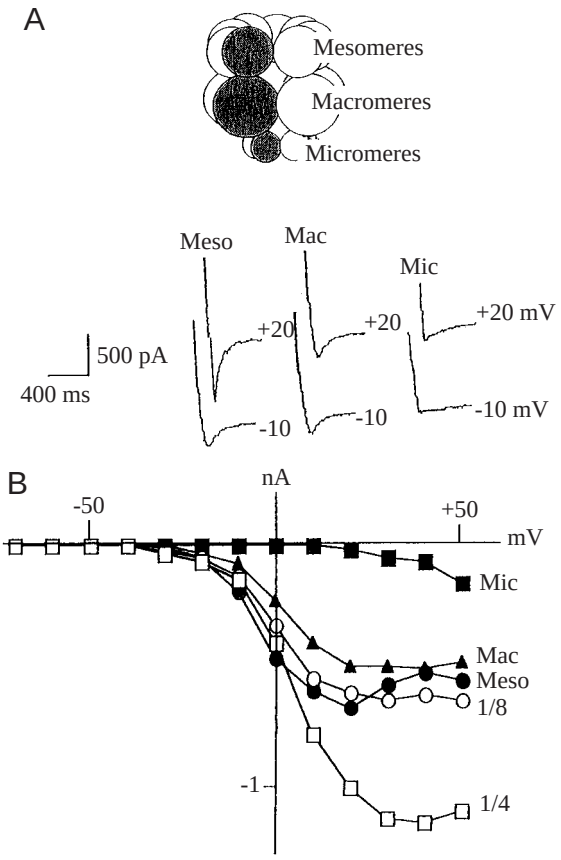

Fig. 7. L-type Ca^{2+} currents in M-phase blastomeres of 16-cell stage sea urchin embryos (A, top). (A) Typical leak-subtracted currents generated at –10 mV (lower traces) and +20 mV (upper traces) from a holding potential of –80 mV. (B) Current/voltage relationships of the L-type Ca^{2+} currents from 4-cell (1/4) and 8-cell (1/8) blastomeres and mesomeres (Meso), macromeres (Mac) and micromeres (Mic). Values are means of five measurements; error bars are omitted for clarity. (Taken from Dale et al., 1997, with permission.)

produce smaller cells posteriorly. These unequal divisions are preceded by migration of the nucleus, led by one centrosome, in the posterior direction, where a unique structure designated the centrosome-attracting body (CAB) is present (Hibino et al., 1998). The CAB, which is visible after ooplasmic segregation and is inhibited by treatment with SDS, is essential for nuclear migration, which is accomplished by the shortening of microtuble bundles formed between the centrosome and the CAB (Nishikata et al., 1999).

Neither a CAB nor CAB-like structures have been found in sea urchin embryos. We stained the endoplasmic reticulum (ER) by microinjecting a saturated solution of the fluorescent dye, dicarbocyanine $DiIC_{16}$ in soybean oil according to the published method (Terasaki and Jaffe, 1991). The dye spreads from the oil drop into ER membranes throughout the egg, but not into other organelles. The stained ER has the appearance of a tubular membrane network in the cortex of sea urchin blastomeres (Fig. 8A2′). In 16-cell stage embryos, there is a considerable accumulation of ER in the micromere, although a meshwork of ER is visible in the cortical layer of every blastomere (Fig. 8A1, A2, A2′). The accumulation of ER is intially observed in the vegetal half of 4-cell stage blastomeres (Fig. 8B2, B3), and subsequently accumulates at the vegetal pole of the 8-cell blastomere (arrowheads) although it is not present in another adjacent blastomere (arrows in Fig. 8C2, C3). If the embryo is treated with SDS during the 4-cell stage to inhibit the unequal cleavage at the fourth division, the accumulation of ER is also inhibited. Fig. 8D shows the equal size of blastomeres and equal distribution of ER in a quarter embryo at the 16-cell stage. This suggests that the local accumulation of ER in the vegetal half of the 4-cell stage blastomeres is the first step in the process that gives rise to the micromeres.

Micromeres have a high intracellular Ca^{2+} concentration

The cortical endoplasmic reticulum of sea urchin eggs can release and take up Ca^{2+} (Terasaki and Sardet, 1991). Using the acetoxymethyl esters of Fura-2 (Fura-2/AM), Ca^{2+} concentrations in blastomeres from the 2- to 16-cell stages

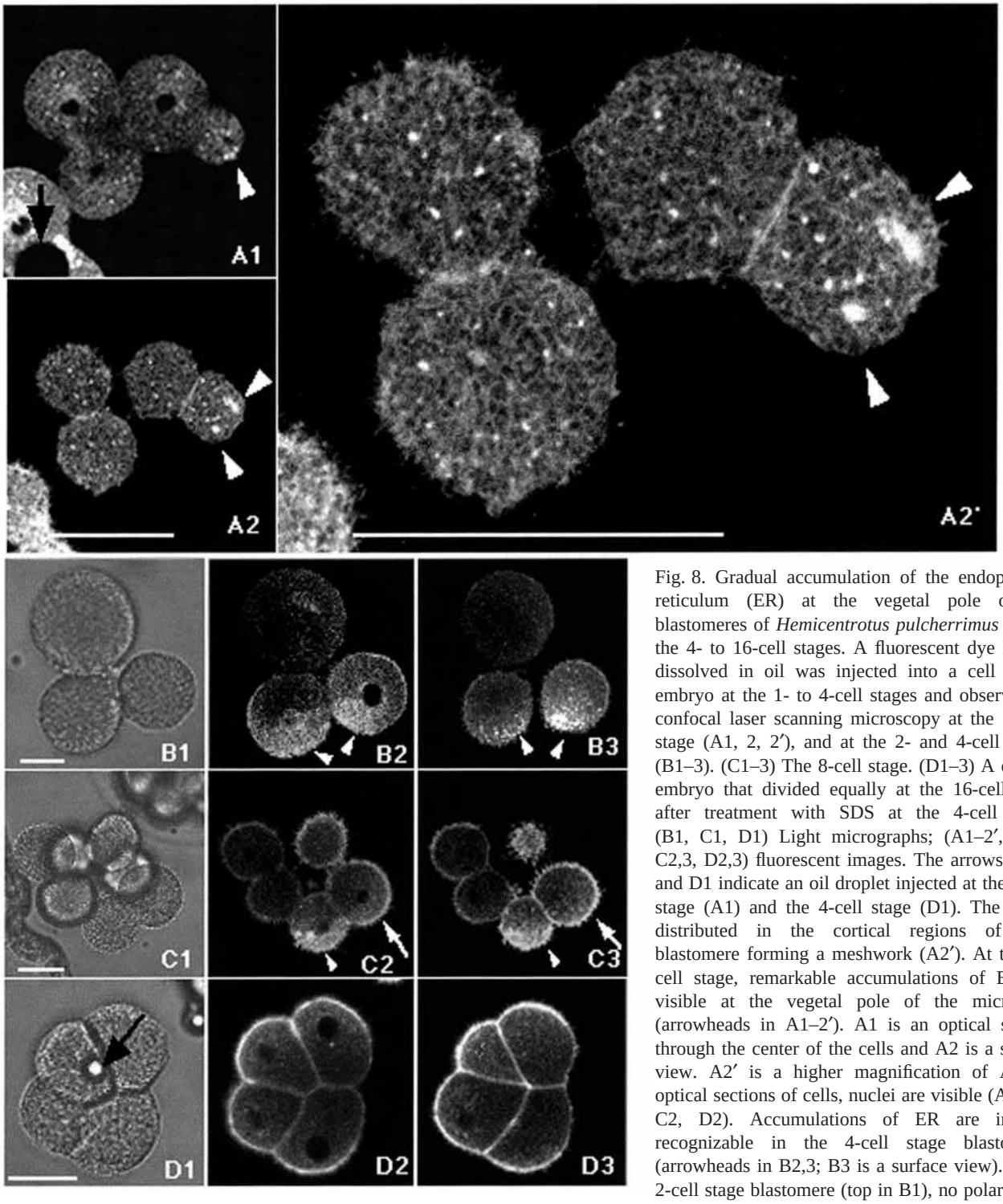

Fig. 8. Gradual accumulation of the endoplasmic reticulum (ER) at the vegetal pole of the blastomeres of *Hemicentrotus pulcherrimus* during the 4- to 16-cell stages. A fluorescent dye $DiIC_{16}$ dissolved in oil was injected into a cell in the embryo at the 1- to 4-cell stages and observed by confocal laser scanning microscopy at the 16-cell stage (A1, 2, 2′), and at the 2- and 4-cell stages (B1–3). (C1–3) The 8-cell stage. (D1–3) A quarter embryo that divided equally at the 16-cell stage after treatment with SDS at the 4-cell stage. (B1, C1, D1) Light micrographs; (A1–2′, B2,3, C2,3, D2,3) fluorescent images. The arrows in A1 and D1 indicate an oil droplet injected at the 2-cell stage (A1) and the 4-cell stage (D1). The ER is distributed in the cortical regions of each blastomere forming a meshwork (A2′). At the 16-cell stage, remarkable accumulations of ER are visible at the vegetal pole of the micromere (arrowheads in A1–2′). A1 is an optical section through the center of the cells and A2 is a surface view. A2′ is a higher magnification of A2. In optical sections of cells, nuclei are visible (A1, B2, C2, D2). Accumulations of ER are initially recognizable in the 4-cell stage blastomeres (arrowheads in B2,3; B3 is a surface view). In the 2-cell stage blastomere (top in B1), no polarization or accumulation of ER is seen (B2,3). At the 8-cell stage (C1), one pair of sister cells can be seen (bottom two cells), focussed on the nuclei in C2 and at the cell surface in C3. Accumulations of ER are visible in one cell (arrowhead) but not in the sister cell (arrow). In the blastomeres equally divided at the 16-cell stage (D1), no accumulation of ER is detected (D2,3). Scale bars, 50 μm.

were compared. Fura-2/AM is a cell-permeant dye that becomes impermeant after being hydrolysed by esterase within the cell. The Ca^{2+} concentration can be obtained as a relative value by calculating the ratio of fluorescence intensity at 510 nm emitted from dye activated at two wavelengths, 340 and 380 nm. Thus the size and thickness of cells do not affect the measurements.

Embryos were removed from their fertilization envelopes and blastomeres were separated at the 4-cell stage by placing embryos in Ca^{2+}-deficient sea water and then allowing them to

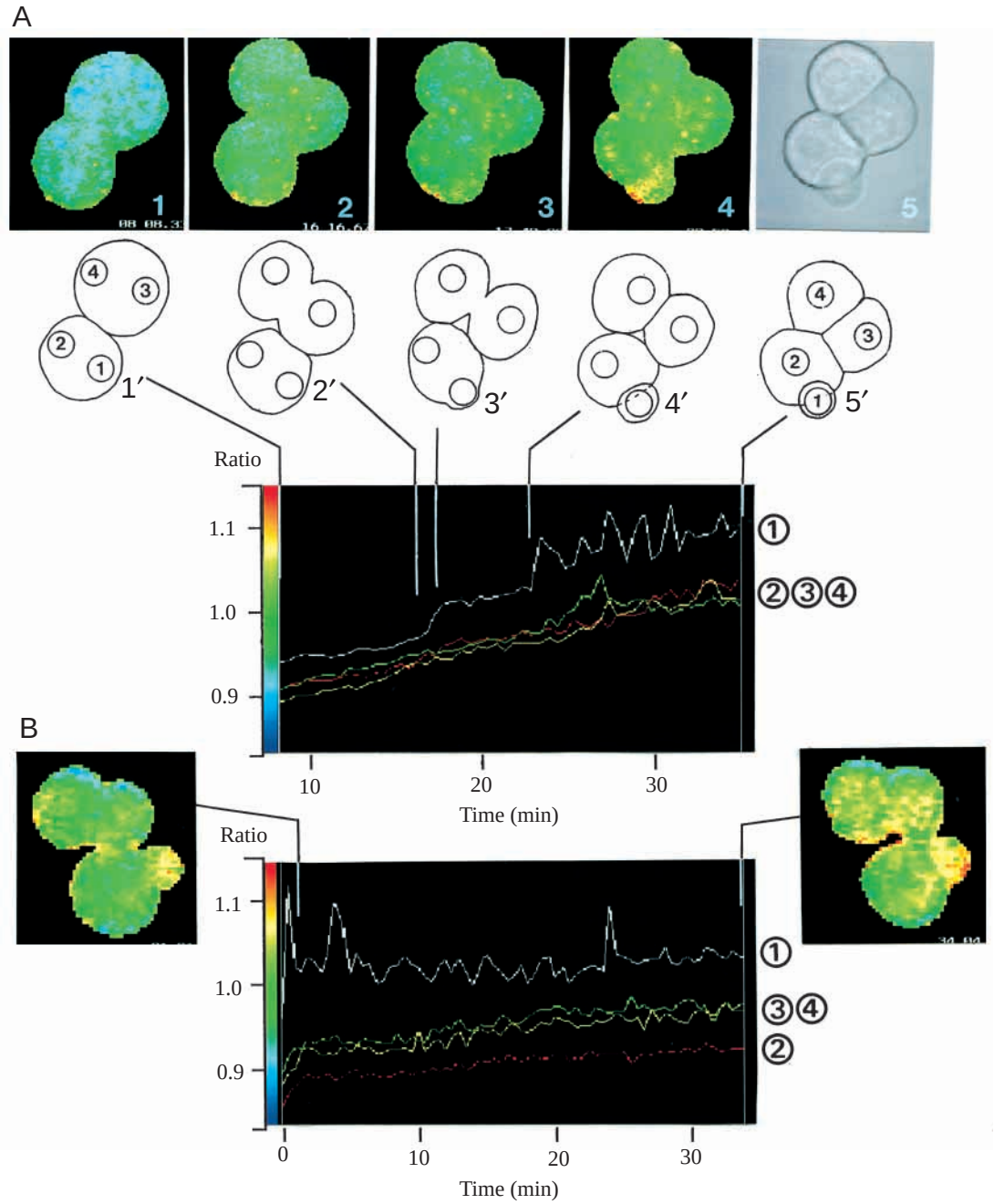

Fig. 9. Relative intracellular Ca^{2+} concentration ($[Ca^{2+}]_i$) in the 16-cell stage blastomeres of *Pseudocentrotus depressus*. The ratios of fluorescence intensity (relative to $[Ca^{2+}]_i$) emitted at two excitation wavelengths were measured in blastomeres loaded with Fura-2/AM (acetoxymethyl esters of Fura-2), using a fluorescence ratio imaging system, ARGUS/HiSCA (Hamamatsu Photonics). Measurements were carried out on a quarter embryo at 30 s intervals from the 8- to 16-cell stages for 35 min (A) and another quarter embryo during the 16-cell stage for 34 min (B). One cell cycle is approximately 38 min. (A) Upper row shows ratio images at various stages (1–4) and a light micrograph of the embryo at the end of the measurement (5). Stages shown are late in the 8-cell stage (1,1′), when furrowing to form the mesomeres has started (2,2′), as the micromere region bulges out (3,3′), when the fourth cleavage is completed (4,4′). By the end of the measurement, the interphase nuclei are still visible (5,5′). The drawings 1′–5′ show the cell shapes corresponding to stages 1–5 and the fluorescence ratios of the numbered blastomeres 1–4 are shown in the graph below: 1, the micromere (white line); 2, the macromere (red line); 3 and 4, two mesomeres (yellow and green lines). The record in A is shown from 8 min after measurements were begun. The $[Ca^{2+}]_i$ of the micromere rises as furrowing is initiated. Ca^{2+} oscillations are detected after the completion of furrowing. (B) Measurements were carried out from early in the 16-cell stage until the end of this stage (the ratio image at 34 min shown on the right of the Fig. shows initiation of the cleavage furrow in the meso- and macromeres). The numbers 1–4 and the related coloured lines indicate the same blastomeres as shown in A. The $[Ca^{2+}]_i$ of the micromere (white line) is higher than that of other blastomeres. Ca^{2+} oscillations usually become quiescent in the later processes of the cell cycle (NBD-cleavage).

Table 2. *Relative Ca^{2+} concentrations in 16-cell stage sea urchin blastomeres*

Species	Number of quarter embryos	mic/mac	meso/mac	meso/meso
Normal embryos				
Unloaded				
Hemicentrotus pulcherrimus	10	0.99±0.003	1.00±0.003	1.01±0.003
Fura-2/AM loaded				
Hemicentrotus pulcherrimus	20	1.14±0.018*	1.02±0.004	1.02±0.004
Pseudocentrotus depressus	24	1.10±0.010*	1.00±0.004	1.00±0.002

	Number of quarter embryos	Ratio between sister blastomeres in quarter embryos
SDS-treated embryos		
Hemicentrotus pulcherrimus	16	1.01±0.003
Pseudocentrotus depressus	8	1.02±0.004

'A quarter embryo' consists of two mesomeres, one macromere and one micromere, which develop from an isolated 4-cell stage blastomere.

mic, micromere; mac, macromere; meso, mesomere; Fura-2/AM, acetoxymethyl ester(AM) of Fura-2, a permeant Ca^{2+} reagent; SDS, sodium dodecyl sulphate, which was used to produce equally sized blastomeres at the 16-cell stage. Values are means ± S.E.M.

*Significantly different from ratios in meso/mac and meso/meso (P<<0.05; by Student's t-test).

develop in normal sea water. This procedure results in the formation of many 'quarter-embryos' consisting of two mesomeres, one macromere and one micromere (Fig. 4). Fura-2/AM was loaded into the 4-cell stage blastomeres and ratio-imaging measurements were carried out at 30 s intervals over a period of 40 min (one division cycle takes 35–40 min) (Fig. 9A,B). Since the fluorescent ratios increase in every blastomere within 40 min of loading, measurements were usually carried out 1 h or more after loading.

In Fig. 9, the ratio in the area of the micromere that was measured, blastomere 1 (indicated by a white line) increases as furrowing begins (Fig. 9A3, 3′) and is maintained at a higher level than that of the other blastomeres, i.e. blastomere 2 for the macromere, and 3 and 4 for the mesomeres during the 16-cell stage (Fig. 9B). Relative Ca^{2+} concentrations were measured as the ratio between two blastomeres so that micromere was compared with macromere, mesomere with macromere and mesomere with mesomere. In the case of natural embryos, i.e. unloaded embryos, the ratios between all blastomere pairs measured was close to 1.0, which means there is no difference between the three types of blastomeres in the ratio of fluorescence intensity excited at two wavelengths. In embryos loaded with Fura-2/AM, the fluorescence intensity ratio of micromere to macromere is significantly higher than 1.0 (1.14±0.018 for *Hemicentrotus pulcherrimus* and 1.10±0.010 for *Pseudocentrotus depressus*; these values are significantly different from the ratios in mesomere/macromere and mesomere/mesomere pairs (P<<0.05), but all other blastomeres have almost the same intracellular calcium concentration (Table 2).

Just before furrowing at the fourth division, there is an elevation of $[Ca^{2+}]_i$ in the small area at the vegetal pole of the 8-cell blastomere, from which micromeres are liberated (Fig. 9A2, 2′ and A3, 3′). As previously stated, SDS-treated embryos divide equally at the fourth division and fail to make either a larval skeleton or an archenteron. In the blastomeres of such embryos, no accumulation of ER is seen (Fig. 8D) and $[Ca^{2+}]_i$ in all 16-cell stage blastomeres are similar (Table 2). It is interesting that in normal embryos, ER accumulation is detected from the 4-cell stage, while a high $[Ca^{2+}]_i$ is detected later, just as furrowing is initiated at the fourth division (Fig. 9A3, 3′).

Ca^{2+} oscillation in the micromeres

Repeated elevations of $[Ca^{2+}]_i$ are measured after the fourth cleavage (Fig. 9A4, 4′–A5, 5′) and then the levels stabilize in the later stages of the mitotic cycle (Fig. 9B). The intervals between peaks of $[Ca^{2+}]_i$ range between approximately 30 s and 60 s. Oscillations do not occur in Ca^{2+}-deficient sea water and are evoked by the addition of Ca^{2+} ions into the bathing medium (data not shown), suggesting that Ca^{2+} influx may initiate the Ca^{2+} oscillations. Since L-type calcium channels are absent from the micromeres (Fig. 7, Table 1), other types of Ca^{2+} channels may be involved in the initiation of these Ca^{2+} oscillations.

Ca^{2+} in fertilization, cell division and gene expression

The rise in $[Ca^{2+}]_i$ during fertilization of sea urchin eggs is caused by an influx of Ca^{2+} (Paul and Johnston, 1978) and release from intracellular stores (Shen and Buck, 1993). Two intracellular Ca^{2+} release mechanisms regulated by inositol triphosphate (IP_3) and ryanodine have been identified in many somatic cell types (Berridge, 1993). Pharmacological studies (Sardet et al., 1992; Livingston and Wilt, 1992; Livingston and Wilt, 1995) and immunohistochemical studies using antibodies against ryanodine receptors (McPherson et al., 1992) and IP_3 receptors (Parys et al., 1994) have shown that sea urchin eggs

contain both mechanisms. Transients in $[Ca^{2+}]_i$ control cell cycle progression by translational and post-translational regulation of the cell cycle control proteins pp34 and cyclin (Whitaker and Patel, 1990).

Ca^{2+} oscillations accompany fertilization in many animals including mammals, amphibia, ascidians and nemertean worms (Miyazaki et al., 1993; Kubota et al., 1993; Speksnijder et al., 1989; Stricker, 1996; Stricker et al., 1998), although distinct repetitive calcium waves after fertilization have not been observed in sea urchins. Two intracellular calcium channels have been implicated in different roles during fertilization of ascidians: ryanodine receptors cause capacitance changes, implying a net insertion of membrane in the oocyte surface, while IP_3 receptors trigger sustained $[Ca^{2+}]_i$ oscillations (Albrieux et al., 1997). In sea urchins, the ryanodine receptors localized in the cortical region of mature eggs are lost after the cortical exocytosis at fertilization, suggesting that the ryanodine receptors are linked with insertion of membrane at the egg surface (McPherson et al., 1992).

In nemerteans, microdomains of ER occur during oocyte maturation. These are closely related to Ca^{2+} oscillations after fertilization but are independent of the egg axis (Stricker et al., 1998). In ascidian eggs, in contrast, the calcium oscillations are initiated near the vegetal pole by a cortical pacemaker (Speksnijder, 1992). The calcium oscillations may influence various events after fertilization, including meiotic events and ooplasmic segregation in ascidian eggs, and mitotic events in sea urchin eggs; however, the physiological role of Ca^{2+} oscillations in embryonic cells is unclear, although in mammalian cells in culture, $[Ca^{2+}]_i$ oscillations and their frequency have been shown to be specific for gene activation (Dolmetsch et al., 1998; Li et al., 1998).

Vegetalization and Ca^{2+}

Lithium chloride vegetalizes sea urchin embryos, i.e. transforms many more cells to endoderm than occurs in normal embryos (Nocente-McGrath et al., 1991), by blocking signalling through the IP_3-pathway (Livingston and Wilt, 1990; Livingston and Wilt, 1992; Livingston and Wilt, 1995). This action is effective not only on the A–V axis of sea urchin but also on the ventral–dorsal axis of amphibian embryos. Lithium chloride is known to interfere with the intracellular Ca^{2+} concentration via the IP_3-signalling pathway and to regulate gene expression in the nucleus (Berridge, 1993), although in *Xenopus laevis* embryos it has recently been proposed that lithium chloride acts through inhibition of glycogen synthetase kinase-3β (GSK-3β), a member of the Wnt signalling pathway, which regulates cell fate determination in a number of diverse organisms including *Dictyostelium discoideum*, *Drosophila melanogaster* and *Xenopus laevis* (Klein and Melton, 1996). In the absence of a Wnt signal, GSK-3 negatively regulates the Wnt signalling pathway by phosphorylating β-catenin, which causes the breakdown of β-catenin. Overexpression of β-catenin causes vegetalization of sea urchin embryos and the lithium chloride treatment enhances the accumulation of β-catenin in the nuclei of vegetal cells (Wikramanayake et al., 1998). The function of β-catenin is thought to be mediated through direct association with transcription factors and the accumulation of this complex in the nucleus (Cavallo et al., 1997). The activity of TCF, a β-catenin binding transcriptional regulator, affects specification along the A–V axis between fertilization and the 60-cell stage (Vonica et al., 2000). According to Logan et al., 1999, β-catenin is initially recognized in the cytoplasm of the 16-cell stage micromeres of sea urchin embryos, and then, after the fifth division, high levels of cytoplasmic and nuclear β-catenin are detected in both the small and large micromeres while lower levels of β-catenin are present in the nuclei of the macromere descendants. It is not known, however, how the β-catenin autonomously increases and localizes in the vegetal cells.

The role of Ca^{2+} in the specification of micromeres and vegetal cell fates

It has been suggested that two functions of the micromeres in *Hemicentrotus pulcherrimus*, skeletogenesis and inductive ability to give rise to the endoderm, are acquired by unequal division at the fourth cleavage (Tanaka, 1976). We have found high $[Ca^{2+}]_i$ and the presence of Ca^{2+} oscillations associated with the micromeres (Table 2, Fig. 9). It is, however, pointless to seek the causes of gastrulation and skeletogenesis in the micromeres, since it is a lengthy and complex process to specify the endodermal cells (gastrulation) and mesodermal cells (skeletogenesis), including complicated regulative cellular interactions (Ettensohn and McClay, 1988; Ettensohn, 1990). For example, a gene for spicule matrix protein SM30 is transcribed in cultured micromeres as well as in intact embryos but the transcripts of SM30 are first detectable at around the onset of spicule formation (Kitajima et al., 1996). In the case of Endo 16, which encodes the surface protein of the archenteron cells, the gene is activated at the early blastula stage, before gastrulation, but not at the 16-cell stage (Nocente-McGrath et al., 1989). To my knowledge, the micromere-specific gene expression has not been identified (Giudice, 1995; Giudice, 1999).

A novel tyrosine kinase, which phosphorylates and activates GSK3β to direct cell fate specification, is found in *Dictyostelium discoidium* (Kim et al., 1999). In the sea urchin, β-catenin initially appears in the cytoplasm of micromeres at the 16-cell stage and accumulates in the nuclei at the 32-cell stage (Logan et al., 1999); however, transcripts of sea urchin homolog of GSK3β are expressed from unfertilized eggs to blastula in every embryonic cell (Emily-Fenouil et al., 1998). High $[Ca^{2+}]_i$ is first detectable at the time when the micromeres are about to constrict. At present we have no evidence to link the behaviour of β-catenin and $[Ca^{2+}]_i$; however, high $[Ca^{2+}]_i$ may regulate the localization of β-catenin through phosphorylation of GSK3β by a Ca^{2+}-sensitive protein kinase or tyrosine kinase, which has not been identified in sea urchin embryos.

Autonomous formation of micromeres with high $[Ca^{2+}]_i$

High $[Ca^{2+}]_i$ and $[Ca^{2+}]_i$ oscillations are first detectable when the micromeres are about to constrict, though a Ca^{2+} reservoir, in the form of the ER, accumulates earlier. Since the high $[Ca^{2+}]_i$ and $[Ca^{2+}]_i$ oscillations are inhibited by 2-aminoethoxy diphenylborate (2APB), a modulator of IP_3-induced Ca^{2+} (Maruyama et al., 1997), both may be attenuated by release from the ER Ca^{2+} reservoir. The $[Ca^{2+}]_i$ oscillations at fertilization are initiated by Ca^{2+} influx following sperm entry. The present study suggest that voltage-dependent L-type Ca^{2+} channels are absent in micromeres (Fig. 7, Table 1). When the 8-cell stage blastomeres are exposed to a blocker of Ca^{2+} influx, SKF 96356 (Cabello and Shilling, 1993), the blastomeres cannot initiate furrowing, $[Ca^{2+}]_i$ increases or $[Ca^{2+}]_i$ oscillations. When applied after the elevation of $[Ca^{2+}]_i$ in the micromeres, SKF 96356 does not affect on the level of $[Ca^{2+}]_i$, but $[Ca^{2+}]_i$ oscillations are not detected (data not shown). The initial influx of Ca^{2+} may result from activation of a calcium channel that is sensitive to stretch-stress produced by the cleavage furrowing (Lee et al., 1999; Mitsuyama et al., 1999). In this way, the micromeres are specified to have high $[Ca^{2+}]_i$ or $[Ca^{2+}]_i$ oscillations subsequent to autonomous specification of their surface membrane and cytoplasmic components, which are derived from eggs by autonomous cortical movements and cleavages.

I thank Drs Y. Kudo and K. Mikoshiba for their valuable suggestions on calcium measurements and also Ms Y. Koyama and Dr M. Abe for their collaborations on calcium data in the present paper. I greatly appreciate Dr R. Hill for critically reading the manuscript and for improving the English. My research on calcium was supported by the Fund for Special Research Projects 1997 at Tokyo Metropolitan University.

References

Albrieux, M., Sardet, C. and Villaz, M. (1997). The two intracellular Ca^{2+} release channels, ryanodine receptor and inositol 1,4,5-triphosphate receptor, play different roles during fertilization in ascidians. *Dev. Biol*. **189**, 174–185.

Angerer, L. M., Oleksyn, D. W., Logan, C. Y., McClay, D. R., Dale, L. and Angere, R. C. (2000). A BMP pathway regulates cell fate allocation along the sea urchin animal–vegetal embryonic axis. *Development* **127,** 1105–1114.

Belanger, A. M., and Rustad, R. C. (1972). Movements of echinochrome granules during the early development of sea urchin eggs. *Nature New Biol*. **239**, 81–83.

Berridge, M. J. (1993). Inositol triphosphate and calcium signalling. *Nature* **361**, 315–325.

Boveri, T. (1901). Uber die Polaritate des Seeigel-Eies. *Verh. Phys.-Med. Ges. Wurzburg* **34**, 145–176.

Cabello, O. A. and Schilling, W. P. (1993). Vectorial Ca^{2+} flux from the extracellular space to the endoplasmic reticulum via a restricted cytoplasmic component regulates inositol 1,4,5-triphosphate-stimulated release from internal stores in vascular endothelial cells. *Biochem. J.* **295**, 357–366.

Cavallo, R., Rubenstein, D. and Peifer, M. (1997). Armadillo and dTce: a marriage made in the nucleus. *Curr. Opin. Genet. Dev*. **7**, 459–466.

Dale, B., Yazaki, I. and Tosti, E. (1997). Polarized distribution of L-type calcium channels in early sea urchin embryos. *Am. J. Physiol*. **273**, C822–825.

Dan, K. (1954). The cortical movement in *Arbacia punctulata* eggs through cleavage cycles. *Embryologia* **2**, 115–122.

Dan, K. (1960). Cyto-embryology of echinoderms and amphibia. *Int. Rev. Cytol*. **9**, 321–367.

Dan, K. (1979). Studies on unequal cleavage in sea urchins I. Migration of the nuclei to the vegetal pole. *Dev. Growth Differ*. **21**, 527–535.

Dan, K., Endo, S. and Uemura, I. (1983). Studies on unequal cleavage in sea urchins II. Surface differentiation and the direction of nuclear migration. *Dev. Growth Differ*. **25**, 227–237.

Davidson, H. (1989). Lineage-specific gene expression and the regulative capacities of the sea urchin embryo: a proposed mechanism. *Development* **105**, 421–445.

Dolmetsch, R. E., Xu, K. and Lewis, R. S. (1998). Calcium oscillations increase the efficiency and specificity of gene expression. *Nature* **392**, 933–936.

Driesch, H. (1900). Die isolirten Blastomeren des Echinidenkeimes. *Arch. f. Entw. Mech.* **10**, 361–410.

Emily-Fenouil, F., Ghiglione, C., Lhomond, G., Lepage, T. and Gache, C. (1998). GSK3β/shaggy mediates patterning along the animal–vegetal axis of the sea urchin embryo. *Development* **125**, 2489–2498.

Ettensohn, C. A. and McClay, D. R. (1988). Cell lineage conversion in the sea urchin embryo. *Dev. Biol*. **125**, 396–409.

Ettensohn, C. A. (1990). Cell interactions in the sea urchin embryo studied by fluorescence photoablation. *Science* **248**, 247–249**.**

Giudice, G. (1995). Genes of the sea urchin embryo: an annotated list as of December 1994. *Dev. Growth Differ*. **37**, 221–242.

Giudice, G. (1999). Genes and their products in sea urchin development. *Curr. Top. Dev. Biol*. **45**, 41–116.

Hibino, T., Nishikata, T., and Nishida, H. (1998). Centrosome-attracting body: a novel structure closely related to unequal cleavages in the ascidian embryo. *Dev. Growth Differ*. **40**, 85–95.

Horstadius, S. (1939). The mechanism of sea urchin development, studied by operative methods. *Biol. Rev. Camb. Phil. Soc*. **14**, 132–179.

Kim, L., Liu, J. and Kimmel, A. R. (1999). The novel tyrosine kinase ZAK1 activates GSK3 to direct cell fate specification. *Cell* **99**, 399–408.

Kitajima, T., Tomita, M., Killian, C. E., Akasaka, K. and Wilt, F. H. (1996). Expression of spicule matrix protein gene SM30 in embryonic and adult mineralized tissues of sea urchin *Hemicentrotus pulcherrimus. Dev. Growth Differ*. **38**, 687–695.

Klein, P. S. and Melton, D. A. (1996). A molecular mechanism for the effect of lithium on development. *Proc. Natl. Acad. Sci. USA* **93**, 8455–8459.

Kubota, H. Y., Yoshimoto, Y. and Hiramoto, Y. (1993). Oscillation of intracellular free calcium in cleaving and cleavage-arrested embryos of *Xenopus laevis*. *Dev. Biol.* **160**, 512–518.

Kuraishi, R. (1989). Structural and functional polarity of starfish blastomeres. *Dev. Biol.* **136**, 304–310.

Lee, J., Ishihara, A., Oxford, G., Johnson, B. and Jacobson, K. (1999). Regulation of cell movement is mediated by stretch-activated calcium channels. *Nature* **400**, 382–386.

Li, W.-h., Liopis, J., Whiteney, M., Zlokarnik, G. and Tsien, R.

Y. (1998). Cell-permeant caged InsP3 ester shows that Ca^{2+} spike frequency can optimize gene expression. *Nature* **392**, 936–941.

Livingston, B. T. and Wilt, F. H. (1990). Range and stability of cell fate determination in isolated sea urchin blastomeres. *Development* **108**, 403–410.

Livingston, B. T. and Wilt, F. H. (1992). Phorbol esters alter cell fate during development of sea urchin embryos. *J. Cell Biol*. **119**, 1641–1648.

Livingston, B. T. and Wilt, F. H. (1995). Injection of myo-inositol reverses the effects of lithium on sea urchin blastomeres. *Dev. Growth Differ*. **37**, 539–543.

Logan, C. Y., Miller, J. R., Ferkowicz, M. J. and McClay, D. R. (1999). Nuclear β-catenin is required to specify vegetal cell fates in the sea urchin embryo. *Development* **126**, 345–357

Maruyama, Y. K., Nakaseko, Y. and Yagi, S. (1985). Localization of cytoplasmic determinants responsible for primary mesenchyme formation and gastrulation in the unfertilized eggs of the sea urchin *Hemicentrotus pulcherrimus*. *J. Exp. Zool*. **236**, 155–163.

McPherson, S. M., McPherson, P. S., Mathews, L., Cambell, K. P. and Longo, F. J. (1992). Cortical localization of a calcium release channel in sea urchin eggs. *J. Cell Biol.* **116**, 1111–1121.

Mitsuyama, F., Sawai, T., Carafoli, E., Furuichi, T. and Mikoshiba, K. (1999). Microinjection of Ca^{2+} store-enriched microsome fractions to dividing newt eggs induces extra-cleavage furrow via inositol 1,4,5-triphosphate-induced Ca^{2+} release. *Dev. Biol*. **214**, 160–167.

Miyazaki, S., Shirakawa, H., Nakada, K. and Honda, Y. (1993). Essential role of the inositol 1,4,5-triphosphate receptor Ca^{2+} release channel in Ca^{2+} waves and Ca^{2+} oscillations at fertilization of mammalian eggs. *Dev. Biol*. **158**, 62–78.

Nishikata, T., Hibino, T. and Nishida, H. (1999). The centrosome-attracting body, microtuble system, and posterior egg cytoplasm are involved in positioning of cleavage planes in the ascidian embryo. *Dev. Biol*. **209**, 72–85

Nocente-McGrath, C., Brenner, C. A. and Ernst, S. G. (1989). Endo 16, a lineage specific protein of the sea urchin embryo, is first expressed just prior to gastrulation. *Dev. Biol.* **136**, 264–272.

Nocente-McGrath, C., McIsaac, R. and Ernst, S. G. (1991). Altered cell fate in LiCl-treated sea urchin embryos. *Dev. Biol.* **147**, 445–450.

Okazaki, K. (1975). Spicule formation by isolated micromeres of the sea urchin embryo. *Am. Zool*. **15**, 567–581.

Parys, J. B., McPherson, S. M., Mathew, L., Campbell, K. P. and Longo, F. J. (1994). Presence of inositol 1,4,5-triphosphate receptor, calreticulin, and calsequestrin in eggs of sea urchins and *Xenopus laevis. Dev. Biol*. **161**, 466–476.

Paul, M. and Johnston, R. N. (1978). Uptake of Ca^{2+} is one of the earliest response to fertilization of sea urchin eggs. *J. Exp. Zool*. **203**, 143–149.

Ransick, A. and Davidson, E. H. (1993). A complete second gut induced by transplanted micromeres in the sea urchin embryo. *Science* **259**, 1134–1138.

Ransick, A. and Davidson, E. H. (1995). Micromeres are required for normal vegetal plate specification in sea urchin embryos. *Development* **121**, 3215–3222.

Sardet, C., Gillot, I., Ruscher, A., Payan, P., Girard, J. P. and de Renzis, G. (1992). Ryanodine activates sea urchin eggs. *Dev. Growth Differ*. **34**, 37–42.

Shen, S. S. and Buck, W. R. (1993). Source of calcium in sea urchin eggs during the fertilization response. *Dev. Biol.* **157**, 157–169.

Sherwood, D. R. and McClay, D. R. (1999). LvNotch signaling mediates secondary mesenchyme specification in the sea urchin embryo. *Development* **126**, 1703–1713.

Speksnijder, J. E., Corson, D. W., Sardet, C. and Jaffe, L. F. (1989). Free calcium pulse following fertilization in the ascidian egg. *Dev. Biol.* **135**, 182–192.

Speksnijder, J. E. (1992). The repetitive calcium waves in the fertilized ascidian egg are initiated near the vegetal pole by a cortical pacemaker. *Dev. Biol.* **153**, 259–271.

Stricker, S. A. (1996). Repetitive calcium waves induced by fertilization in the nemertean worm *Cerebratulus lacteus. Dev. Biol.* **176**, 243–263.

Stricker, S. A., Silva, R. and Smythe, T. (1998). Calcium and endoplasmic reticulum dynamics during oocyte maturation and fertilization in the marine worm *Cerebratulus lacteus*. *Dev. Biol*. **203**, 305–322.

Tanaka, Y. (1976). Effects of the surfactants on the cleavage and further development of the sea urchin embryos I. The inhibition of micromere formation at the fourth cleavage. *Dev. Growth Differ*. **18**, 113–122.

Tanaka, Y. (1979). Effects of the surfactants on the cleavage and further development of the sea urchin embryos II. Disturbance in the arrangement of cortical vesicles and change in cortical appearance. *Dev. Growth Differ*. **21**, 331–342.

Terasaki, M. and Jaffe, L. A. (1991). Organization of the sea urchin egg endoplasmic reticulum and its reorganization at fertilization. *J. Cell Biol*. **114**, 929–940.

Terasaki, M. and Sardet, C. (1991). Demonstration of calcium uptake and release by sea urchin egg cortical endoplasmic reticulum. *J. Cell Biol*. **115**, 1031–1037.

Vonica, A., Weng, W. M., Gumbiner, B. M. and Venuti, J. M. (2000). TCF is the nuclear effector of the β-catenin signal that patterns the sea urchin animal–vegetal axis. *Dev. Biol.* **207**, 230–243.

Whitaker, M. and Patel, R. (1990). Calcium and cell cycle control. *Development* **108**, 525–542.

Wikramanayake, A. H., Huang, L. and Klein, W. H. (1998). β-catenin is essential for patterning the maternally specified animal–vegetal axis in the sea urchin embryo. *Proc. Natl. Acad. Sci. USA* **95**, 9343–9348.

Yazaki, I. (1984). The egg originated and local distribution of the surface of sea-urchin embryo cells detected by immuno-fluorescence. *Acta Embryo. Morphol. Exp.* **5**, 3–22.

Yazaki, I. and Uemura, I. (1989). Immunocytochemical evidence for the presence of two domains in the plasma membrane of sea urchin blastomeres. *Roux's Arch Dev. Biol*. **198**, 179–184.

Yazaki, I. (1991). Polarization of the surface membrane and cortical layer of sea urchin blastomeres, and its inhibition by cytochalasin B. *Dev. Growth Differ*. **33**, 267–276.

Yazaki, I., Tosti, E. and Dale, B. (1995). Cytoskeletal elements link calcium channel activity and the cell cycle in early sea urchin embryos. *Development* **121**, 1827–1831.

Yazaki, I., Dale, B. and Tosti, E. (1999). Functional gap junctions in the early sea urchin embryo are located to the vegetal pole. *Dev. Biol.* **212**, 503–510.